

Observation of inverse spin Hall effect in bismuth selenide

Praveen Deorani,¹ Jaesung Son,¹ Karan Banerjee,¹ Nikesh Koirala,² Matthew Brahlek,²
Seongshik Oh,² and Hyunsoo Yang^{1,*}

*¹Department of Electrical and Computer Engineering, National University
of Singapore, 117576, Singapore*

*²Department of Physics & Astronomy, Rutgers Center for Emergent Materials, Institute
for Advanced Materials, Devices and Nanotechnology, The State University of New
Jersey, New Jersey 08854, USA*

Bismuth Selenide (Bi_2Se_3) is a topological insulator exhibiting helical spin polarization and strong spin-orbit coupling. The spin-orbit coupling links the charge current to spin current via the spin Hall effect (SHE). We demonstrate a Bi_2Se_3 spin detector by injecting the pure spin current from a magnetic permalloy layer to a Bi_2Se_3 thin film and detect the inverse SHE in Bi_2Se_3 . The spin Hall angle of Bi_2Se_3 is found to be 0.0093 ± 0.0013 and the spin diffusion length in Bi_2Se_3 to be 6.2 ± 0.15 nm at room temperature. Our results suggest that topological insulators with strong spin-orbit coupling can be used in functional spintronic devices.

In a solid, the spin of an electron is coupled to its momentum via spin-orbit interaction. This coupling is manifested in the direct and inverse spin Hall effect (SHE and ISHE) [1-7], which are the processes of inter-conversion of charge and spin currents. The SHE and ISHE have been observed in many materials, including metals and semiconductors. The generation and detection of spin currents is of key importance in spintronics [8-10]. In particular, the ISHE, which converts the spin current into a charge electromotive force (emf), can be used as a powerful detection mechanism for spin currents.

Topological insulators (TI) are a new quantum state of matter where non trivial topology of bulk bands are manifested in gapless spin polarized surface states [11-13]. To date, most of the experiments in TIs have focused on the edge or surface state of these materials. In 2D TIs, edge states have been confirmed by conductance quantization in the insulating regime [14], and the helical spin polarization of these states has been detected by transport experiments like the quantum spin Hall effect [15]. In 3D TIs, there have been many studies which employ angle-resolved photoemission spectroscopy (ARPES) to observe the Dirac cones and confirm its non-degenerate nature. Besides that, the spin-resolved ARPES has been conducted to confirm the helical spin polarization in surface states in 3D TIs [16, 17]. The surface state conduction has been confirmed by sample thickness dependence of transport properties [18-20], and by quantum oscillations from the surface state [18, 21-23]. However, spin transport is little studied in TIs because of the difficulties such as impedance mismatch [24] and an expected small spin diffusion length in TIs due to strong spin-orbit coupling [25]. Recently, spin-orbit effects have been observed in TIs, reporting a wide range of spin Hall angle. [26-28]

In this work we report the observation of ISHE in the prototypical 3D TI, Bi_2Se_3 , and demonstrate its feasibility as a spin current detector. We utilize spin pumping from a permalloy (Py) layer to generate spin currents into the Bi_2Se_3 layer, and measure the induced emf signal [6, 29-32]. Spin pumping is free from the impedance mismatch problem [33] and provides high density spin current injection into the Bi_2Se_3 layer. From thickness dependent measurements, the spin Hall angle (θ_{sh}) and spin diffusion length (λ_{sf}) in Bi_2Se_3 thin films are obtained to be 0.0093 ± 0.0013 and 6.22 ± 0.15 nm, respectively, at room temperature (RT). Both the θ_{sh} and λ_{sf} are observed to increase as the temperature decreases.

Bi_2Se_3 thin films were grown on $\text{Al}_2\text{O}_3(0001)$ substrates using custom designed SVTA MOSV-2 MBE system with base pressure less than 3×10^{-10} Torr. 99.999% pure bismuth and selenium sources were placed in Knudsen cells and evaporated to provide stable fluxes. An Inficon BDS-250 XTC/3 Quartz crystal microbalance was used to measure the flux of individual elements. kSA 400 reflection high energy electron diffraction (RHEED) measurement system was used to monitor the crystal quality of Bi_2Se_3 thin films during growth. $\text{Al}_2\text{O}_3(0001)$ substrates were cleaned for 5 minutes using *ex situ* UV/ozone cleaner to remove organic contaminants on the surface and were immediately loaded into the MBE growth chamber afterwards. In the growth chamber, the substrates were heated to 750 °C for 10 minutes in 1×10^{-6} Torr oxygen environment to remove any excess contaminants. The substrates were then cooled to growth temperature of 135 °C, while the sources were heated to desired temperature of 600 °C and 186 °C for Bi and Se, respectively. We employ a two step growth procedure for Bi_2Se_3 thin film growth as reported previously [34]. A seed layer of 3 quintuple layer

Bi_2Se_3 was grown at 135 °C followed by annealing to 220 °C for 10 minutes before depositing rest of the film at 220 °C. Highly crystalline Bi_2Se_3 films were obtained as indicated by sharp streaks and associated Kikuchi lines in the RHEED pattern. The carrier concentration of the Bi_2Se_3 film was obtained from Hall measurements.

The devices were fabricated by the following process. First, a Bi_2Se_3 film is etched using Ar ion milling to the desired thickness, and is patterned into a $800\ \mu\text{m} \times 600\ \mu\text{m}$ film using photolithography and Ar ion milling. Then, a 20 nm Py ($\text{Ni}_{81}\text{Fe}_{19}$) layer is sputter deposited and patterned into a $640\ \mu\text{m} \times 600\ \mu\text{m}$ strip. In the next step, a $600\ \mu\text{m} \times 630\ \mu\text{m} \times 30\ \text{nm}$ SiO_2 layer is deposited to isolate the Py layer. Then, in the last step, Ta (5 nm)/Cu (150 nm) asymmetric coplanar strips (ACPS) and dc probe pads are patterned, and sputter deposited, simultaneously. In the ACPS, the width of signal line is $60\ \mu\text{m}$, the width of ground line is $180\ \mu\text{m}$, and the signal-ground spacing is $30\ \mu\text{m}$.

Figure 1(a) shows the resistivity and the carrier concentration of a 20 quintuple layer (QL; 1 QL \approx 1 nm) Bi_2Se_3 film as a function of temperature. The decrease in the resistance with decreasing temperature is a typical characteristic of Bi_2Se_3 and the surface dominant transport in these films has been previously confirmed by sample thickness dependent studies of transport properties [19, 20]. Figure 1(b) elucidates the spin pumping process. The precessing magnetization M of the ferromagnet gives rise to a spin current J_s from the ferromagnet to a non-magnetic material (Bi_2Se_3). This spin current is detected as a transverse voltage via ISHE in Bi_2Se_3 , given by $V_{\text{ISHE}} \propto J_s \times \sigma$, where σ denotes the spin polarization vector of the spin current. Figure 1(c) shows a schematic of the device with the measurement set-up. The cross-section of the device is shown in Fig. 1(d). For spin pumping induced ISHE measurements, a 15 dBm microwave signal of a

fixed frequency of 3, 4, 5, and 6 GHz ($= \omega/2\pi$) is applied to the asymmetric coplanar strips (ACPS) waveguide using a signal generator (SG) and a dc voltage is measured across the Bi₂Se₃/Py bilayers as a function of the bias field (H_b) applied along the z -direction. For the evaluation of enhancement in the Gilbert damping constant (α), ferromagnetic resonance (FMR) measurements are carried out using a vector network analyzer. Measurements are carried out at different temperatures ranging from 15 to 300 K.

Figure 2(a) shows the measured data of the electromotive force signal in a Bi₂Se₃ (20 nm)/Py device measured at a frequency of 4 GHz. The H_b along the z -direction is swept across the resonance field H_0 , which is related to the applied frequency by Kittel formula, $\omega = \gamma\mu_0\sqrt{H_0(H_0 + M)}$, where γ is the gyromagnetic ratio of a free electron, μ_0 is the permeability of free space, and M is the saturation magnetization of Py. The measured signal originates from three sources; the ISHE in the Bi₂Se₃ layer, the anisotropic magnetoresistance (AMR) of the Py layer, and the anomalous Hall effect (AHE) of the Py layer [6, 35, 36]. The effect of AMR or AHE from the Py layer needs to be eliminated considering that the ISHE signal has a symmetric Lorentzian shape, whereas the signal due to AMR or AHE has an asymmetric Lorentzian shape [6, 35]. Therefore, the measured data are fitted by a sum of symmetric and asymmetric

Lorentzian functions, $V = V_{sym} \frac{\Gamma^2}{\Gamma^2 + (H - H_0)^2} + V_{asym} \frac{\Gamma(H - H_0)}{\Gamma^2 + (H - H_0)^2}$ and the value of

V_{sym} is taken to be the spin pumping induced ISHE signal (V_{ISHE}). It must be noted that spin rectification effects may also contribute to the symmetric part of the signal [37-39].

These effects originate from the AMR of the Py layer, therefore in order to rule out such

a contribution, we perform measurements on a bare Py layer (without Bi₂Se₃). Only a small asymmetric signal but no symmetric signal is observed as shown in Fig. 2(a).

The spin current density induced by spin pumping is given by [40]

$$J_s = \frac{\hbar g_{r\uparrow\downarrow} \gamma^2 h_{rf}^2 \left(M\gamma + \sqrt{M^2\gamma^2 + 4\omega^2} \right)}{8\pi\alpha^2 \left(M^2\gamma^2 + 4\omega^2 \right)} \frac{\lambda_{sf}}{d_{BiSe}} \tanh\left(\frac{d_{BiSe}}{2\lambda_{sf}} \right) \quad (1)$$

where h_{rf} is the rf field amplitude, f is the applied frequency ($\omega = 2\pi f$), λ_{sf} is the spin diffusion length in Bi₂Se₃, and d_{BiSe} is the thickness of the Bi₂Se₃ layer. $g_{r\uparrow\downarrow}$ is the spin mixing conductance of the Bi₂Se₃/Py interface and is a measure of efficiency of spin pumping across the interface [41, 42]. Due to the ISHE in the Bi₂Se₃ layer, this spin current is converted into a charge current with a density given by $J_c = \theta_{sh} (2e/\hbar) J_s$, where θ_{sh} is the spin Hall angle in Bi₂Se₃. For the device width w (see Fig. 1(c)), this charge current $I_c = J_c (wd_{BiSe})$ across the resistance R of the Bi₂Se₃/Py bilayer is detected as an emf, $V_{ISHE} = J_c (wd_{BiSe}) R$. Thus the measured ISHE signal can be written as

$$\frac{V_{ISHE}}{R} = \theta_{sh} w d_{BiSe} \left(\frac{2e}{\hbar} \right) \frac{\hbar g_{r\uparrow\downarrow} \gamma^2 h_{rf}^2 \left(M\gamma + \sqrt{M^2\gamma^2 + 4\omega^2} \right)}{8\pi\alpha^2 \left(M^2\gamma^2 + 4\omega^2 \right)} \frac{\lambda_{sf}}{d_{BiSe}} \tanh\left(\frac{d_{BiSe}}{2\lambda_{sf}} \right). \quad (2)$$

The value of h_{rf} can be estimated used microwave photoresistance measurements [43-45]. Figure 2(b) shows the microwave photoresistance data from a Bi₂Se₃ (20 nm)/Py device at 4 GHz. From these measurements, the cone angle of precession is calculated to be 0.23°, and h_{rf} is estimated to be ~ 1 Oe using the method described in a previous report [44]. It is also noteworthy that the photoresistance signals in our devices are of the same magnitude in both positive and negative H_b , which is in agreement with the equal magnitude of spin pumping induced ISHE signals at $\pm H_b$.

In order to determine the spin Hall angle and spin diffusion length in the Bi_2Se_3 layer, spin pumping induced ISHE measurements were carried out in samples with different thicknesses of the Bi_2Se_3 layer. Figure 2(c) shows the measured value of V_{ISHE}/R for different thicknesses of the Bi_2Se_3 layer, and a corresponding fit by Eq. (2). From the fitting we obtain a value of $\lambda_{sf} = 6.22 \pm 0.15$ nm at room temperature for the spin diffusion length. The fitting also gives us the product $g_{r\uparrow\downarrow}\theta_{sh} = (4.57 \pm 0.12) \times 10^{16} \text{ m}^{-2}$, where $g_{r\uparrow\downarrow}$ can be obtained by using ferromagnetic resonance (FMR) measurements. Since spin pumping is a process in which the precessing magnetization loses energy, the effective Gilbert damping increases due to spin pumping [41, 46]. In Fig. 2(d) the FMR full linewidth measured as a function of frequency is seen to be larger in $\text{Bi}_2\text{Se}_3/\text{Py}$ devices than that in Py devices. The values of α for Py and $\text{Bi}_2\text{Se}_3/\text{Py}$ from the linear fits by the equation $\Delta H = \Delta H_0 + 4\pi\alpha f/\gamma$ are found to be 0.0109 and 0.0122, respectively. The spin mixing conductance is related to the enhancement in effective α via $g_{r\uparrow\downarrow} = 4\pi M d_{\text{Py}} (\Delta\alpha)/(g \mu_B)$. [35, 40] Thus, $g_{r\uparrow\downarrow}$ is found to be $1.514 \times 10^{19} \text{ m}^{-2}$ and θ_{sh} to be 0.0093 ± 0.0013 at room temperature.

It must be noted that recently a very large value of θ_{sh} (2 – 3.5) was reported in Bi_2Se_3 by spin torque ferromagnetic resonance (ST-FMR) measurements in $\text{Bi}_2\text{Se}_3/\text{Py}$ devices [26]. In another similar material, $(\text{Bi}_{0.5}\text{Sb}_{0.5})_2\text{Te}_3$, an even larger θ_{sh} (140 – 425) was reported using spin-orbit switching measurements in $(\text{Bi}_{0.5}\text{Sb}_{0.5})_2\text{Te}_3/(\text{Cr}_{0.08}\text{Bi}_{0.54}\text{Sb}_{0.38})_2\text{Te}_3$ heterostructures [27]. Our value of θ_{sh} in Bi_2Se_3 is much smaller and closer to that in a conventional heavy metal like Pt [30, 47]. One possibility for the discrepancy could be that both ST-FMR and spin-orbit switching measurements involve a current injection through the TI material, in which the spin-

momentum locking mechanism may play an important role in determining θ_{sh} , unlike our spin pumping experiments. It is also possible that the quality of TI films plays a role in the above discrepancy as it is known that TI materials pose challenges in high quality film growth.

We further extended our study to low temperatures. The Bi_2Se_3 thickness dependent measurements of V_{ISHE} were carried out at different temperatures ranging from 15 to 300 K in order to obtain the θ_{sh} and λ_{sf} at each temperature. Figure 3(a) shows the variation of θ_{sh} and λ_{sf} as a function of temperature. Both θ_{sh} and λ_{sf} increase at low temperatures to be $\theta_{sh} = 0.022 \pm 0.0028$ and $\lambda_{sf} = 9.5 \pm 0.35$ nm at 15 K. The increase in λ_{sf} may be related to a decrease in phonon scattering or an increase in the carrier mobility as temperature is lowered. λ_{sf} is related to the spin diffusion time (τ_{sf}) via $\lambda_{sf} = \sqrt{D\tau_{sf}}$, where D is the diffusion constant. D is related to the carrier mobility through Einstein's relation $D = \mu k_B T / e$. The carrier mobility in our Bi_2Se_3 film is found to increase by three times at low temperature [48], thus qualitatively explaining the increase in λ_{sf} at low temperatures.

The spin orbit length (l_{so}) in Bi_2Se_3 was obtained by weak antilocalization measurements. For these measurements the $100 \mu\text{m} \times 20 \mu\text{m}$ films were fabricated by photolithography by Ar ion milling process and the electrical contacts, Ta (5 nm)/Cu (80 nm), were sputter deposited. The electrical resistance of the Bi_2Se_3 films was measured as a function of an out-of-plane magnetic field. We fit this data with the Hikami-Larkin-Nagaoka (HLN) equation along with a quadratic background term [49]

$$\Delta G(B) = -\frac{Ae^2}{\pi h} \left[\psi \left(\frac{\hbar}{4eL^2B} + \frac{1}{2} \right) - \ln \left(\frac{\hbar}{4eL^2B} \right) \right] + \beta B^2 \quad (3)$$

Here, A accounts for contributions from the surface as well as 2D bulk effects, and β is the quadratic coefficient arising from scattering events. ψ is the digamma function, L is the phase coherence length in Bi_2Se_3 , e is the electronic charge, h is Planck constant, and \hbar is the reduced Planck constant. Figure 3(b) shows the measured magnetoconductance (symbols) and the corresponding fit (solid line) by equation (3). From fitting we obtain the value of β to be $-4.32 \times 10^{-9} \Omega^{-1}\text{T}^{-2}$. The β consists of a classical cyclotronic part, and a quantum part that originates from spin orbit scattering and elastic scattering events. The classical part is given by $\beta_c = -\mu_H^2 G_0$, where μ_H is the Hall mobility and G_0 is the zero-field conductance. The quantum part of β is given by

$$\beta_q = -\frac{e^2}{24\pi\hbar} \left[\frac{1}{B_{so} + B_e} \right]^2 + \frac{3e^2}{48\pi\hbar} \left[\frac{1}{(4/3)B_{so} + B_\phi} \right]^2 \quad (4)$$

where $B_{so} = \hbar/(4el_{so}^2)$ and $B_e = \hbar/(4el_e^2)$, with l_{so} and l_e being the spin orbit length and the electron mean free path, respectively. The mobility in our samples was determined to be $61 \text{ cm}^2/\text{V}\cdot\text{sec}$, and G_0 is $5.43 \times 10^{-4} \Omega^{-1}$. Thus the value of β_c is calculated to be $-2.02 \times 10^{-8} \Omega^{-1}\text{T}^{-2}$. Thus, $\beta_q = \beta - \beta_c = 1.58 \times 10^{-8} \Omega^{-1}\text{T}^{-2}$. If we use the electron mean free path, $l_e = 10 \text{ nm}$, the l_{so} can be obtained to be 6.9 nm . The comparable values of l_{so} and λ_{sf} suggest that spin-orbit coupling is the dominant source of spin scattering in the Bi_2Se_3 films.

Bi_2Se_3 films are expected to show a distinct behavior at surface and bulk. For example, the spin-orbit interaction at surface may be different from that in bulk. We thus analyze our data using different values of spin Hall angle for the surface and bulk. Following the method by Ando *et al* [40]. we derive the formula for spin pumping induced V_{ISHE} using different values of spin Hall angle for the surface and bulk,

$$\begin{aligned}
\frac{V_{ISHE}}{R} = & \theta_{sh1} \left(\frac{2e}{\hbar} \right) \frac{\lambda_{sf}}{d_{BiSe}} \operatorname{csch} \left(\frac{d_{BiSe}}{\lambda_{sf}} \right) \left(\cosh \left(\frac{d_{BiSe}}{\lambda_{sf}} \right) - \cosh \left(\frac{d_{BiSe} - d_{surf}}{\lambda_{sf}} \right) \right) J_s^0 \\
& + \theta_{sh2} \left(\frac{2e}{\hbar} \right) \frac{\lambda_{sf}}{d_{BiSe}} \operatorname{csch} \left(\frac{d_{BiSe}}{\lambda_{sf}} \right) \left(\cosh \left(\frac{d_{BiSe} - d_{surf}}{\lambda_{sf}} \right) - \cosh \left(\frac{d_{surf}}{\lambda_{sf}} \right) \right) J_s^0 \\
& + \theta_{sh1} \left(\frac{2e}{\hbar} \right) \frac{\lambda_{sf}}{d_{BiSe}} \operatorname{csch} \left(\frac{d_{BiSe}}{\lambda_{sf}} \right) \left(1 - \cosh \left(\frac{d_{surf}}{\lambda_{sf}} \right) \right) J_s^0, \quad J_s = J_s^0 \frac{\lambda_{sf}}{d_{BiSe}} \tanh \left(\frac{d_{BiSe}}{2\lambda_{sf}} \right)
\end{aligned} \tag{5}$$

where θ_{sh1} and θ_{sh2} are the spin Hall angles at surface and bulk, respectively. d_{surf} is the assumed value of surface thickness and is taken to be 3 nm. The spin Hall angle at opposite surfaces was taken to be of opposite signs. Fitting the measured data, we obtain θ_{sh1} at surface and θ_{sh2} at bulk for each temperature as shown in Fig. 4(a), which does not show any clear distinction between the surface and bulk value. Figure 4(b) shows the λ_{sf} as a function of temperature when different values of spin Hall angle are taken for surface and for bulk.

Our results show the practicability of Bi_2Se_3 as a spin detector. The value of θ_{sh} is higher than that in Si and GaAs, and similar to those obtained for heavy metals such as Pt, Pd, or Ta by spin pumping method [32, 33, 36, 40]. It must be noted that the spin current detection efficiency by ISHE depends not only on θ_{sh} , but also on the resistance of the layer, as $V_{ISHE} \propto \theta_{sh} J_s R$. Since Bi_2Se_3 is a semiconductor, its resistivity is at least an order of magnitude higher than the heavy metals like Pt and hence the spin pumping induced ISHE voltage can be expected to be higher than that in the Pt [50]. Therefore, Bi_2Se_3 can be a viable material for spin detection devices.

This work is partially supported by the Singapore Ministry of Education Academic Research Fund Tier 1 (R-263-000-A75-750), the National Research Foundation, Prime Minister's Office, Singapore under its Competitive Research Programme (CRP Award No. NRF-CRP 4-2008-06), National Science Foundation (NSF DMR-0845464), and Office of Naval Research (ONR N000141210456).

*eleyang@nus.edu.sg

References

- [1] M. I. Dyakonov, and V. I. Perel, *Phys. Lett. A* **35**, 459 (1971).
- [2] J. E. Hirsch, *Phys. Rev. Lett.* **83**, 1834 (1999).
- [3] S. Murakami, N. Nagaosa, and S.-C. Zhang, *Science* **301**, 1348 (2003).
- [4] J. Sinova, D. Culcer, Q. Niu, N. A. Sinitsyn, T. Jungwirth, and A. H. MacDonald, *Phys. Rev. Lett.* **92**, 126603 (2004).
- [5] Y. K. Kato, R. C. Myers, A. C. Gossard, and D. D. Awschalom, *Science* **306**, 1910 (2004).
- [6] E. Saitoh, M. Ueda, H. Miyajima, and G. Tatara, *Appl. Phys. Lett.* **88**, 182509 (2006).
- [7] T. Kimura, Y. Otani, T. Sato, S. Takahashi, and S. Maekawa, *Phys. Rev. Lett.* **98**, 156601 (2007).
- [8] M. Johnson, and R. H. Silsbee, *Phys. Rev. Lett.* **55**, 1790 (1985).
- [9] F. J. Jedema, A. T. Filip, and B. J. van Wees, *Nature* **410**, 345 (2001).
- [10] X. Lou, C. Adelman, S. A. Crooker, E. S. Garlid, J. Zhang, K. S. M. Reddy, S. D. Flexner, C. J. Palmstrom, and P. A. Crowell, *Nat. Phys.* **3**, 197 (2007).
- [11] M. Z. Hasan, and C. L. Kane, *Rev. Mod. Phys.* **82**, 3045 (2010).
- [12] J. E. Moore, *Nature* **464**, 194 (2010).
- [13] X.-L. Qi, and S.-C. Zhang, *Rev. Mod. Phys.* **83**, 1057 (2011).
- [14] M. König, S. Wiedmann, C. Brüne, A. Roth, H. Buhmann, L. W. Molenkamp, X.-L. Qi, and S.-C. Zhang, *Science* **318**, 766 (2007).
- [15] C. Brune, A. Roth, H. Buhmann, E. M. Hankiewicz, L. W. Molenkamp, J. Maciejko, X.-L. Qi, and S.-C. Zhang, *Nat. Phys.* **8**, 485 (2012).
- [16] D. Hsieh, Y. Xia, L. Wray, D. Qian, A. Pal, J. H. Dil, J. Osterwalder, F. Meier, G. Bihlmayer, C. L. Kane *et al.*, *Science* **323**, 919 (2009).
- [17] A. Nishide, A. A. Taskin, Y. Takeichi, T. Okuda, A. Kakizaki, T. Hirahara, K. Nakatsuji, F. Komori, Y. Ando, and I. Matsuda, *Phys. Rev. B* **81**, 041309 (2010).
- [18] A. A. Taskin, Z. Ren, S. Sasaki, K. Segawa, and Y. Ando, *Phys. Rev. Lett.* **107**, 016801 (2011).
- [19] N. Bansal, Y. S. Kim, M. Brahlek, E. Edrey, and S. Oh, *Phys. Rev. Lett.* **109**, 116804 (2012).
- [20] R. Valdés Aguilar, A. V. Stier, W. Liu, L. S. Bilbro, D. K. George, N. Bansal, L. Wu, J. Cerne, A. G. Markelz, S. Oh *et al.*, *Phys. Rev. Lett.* **108**, 087403 (2012).
- [21] Z. Ren, A. A. Taskin, S. Sasaki, K. Segawa, and Y. Ando, *Phys. Rev. B* **82**, 241306 (2010).
- [22] D.-X. Qu, Y. S. Hor, J. Xiong, R. J. Cava, and N. P. Ong, *Science* **329**, 821 (2010).
- [23] J. G. Analytis, R. D. McDonald, S. C. Riggs, J.-H. Chu, G. S. Boebinger, and I. R. Fisher, *Nat. Phys.* **6**, 960 (2010).
- [24] G. Schmidt, D. Ferrand, L. W. Molenkamp, A. T. Filip, and B. J. van Wees, *Phys. Rev. B* **62**, R4790 (2000).
- [25] C. Ojeda-Aristizabal, M. S. Fuhrer, N. P. Butch, J. Paglione, and I. Appelbaum, *Appl. Phys. Lett.* **101**, 023102 (2012).
- [26] A. R. Mellnik, J. S. Lee, A. Richardella, J. L. Grab, P. J. Mintun, M. H. Fischer, A. Vaezi, A. Manchon, E. A. Kim, N. Samarth *et al.*, *Nature* **511**, 449 (2014).

- [27] Y. Fan, P. Upadhyaya, X. Kou, M. Lang, S. Takei, Z. Wang, J. Tang, L. He, L.-T. Chang, M. Montazeri *et al.*, *Nat. Mater.* **13**, 699 (2014).
- [28] Y. Shiomi, K. Nomura, Y. Kajiwara, K. Eto, M. Novak, K. Segawa, Y. Ando, and E. Saitoh, arXiv:1312.7091 (2013).
- [29] K. Ando, Y. Kajiwara, K. Sasage, K. Uchida, and E. Saitoh, *IEEE Trans. Magn.* **46**, 3694 (2010).
- [30] O. Mosendz, V. Vlaminck, J. E. Pearson, F. Y. Fradin, G. E. W. Bauer, S. D. Bader, and A. Hoffmann, *Phys. Rev. B* **82**, 214403 (2010).
- [31] S. S. Mukherjee, P. Deorani, J. H. Kwon, and H. Yang, *Phys. Rev. B* **85**, 094416 (2012).
- [32] P. Deorani, and H. Yang, *Appl. Phys. Lett.* **103**, 232408 (2013).
- [33] K. Ando, S. Takahashi, J. Ieda, H. Kurebayashi, T. Trypiniotis, C. H. W. Barnes, S. Maekawa, and E. Saitoh, *Nat. Mater.* **10**, 655 (2011).
- [34] N. Bansal, Y. S. Kim, E. Edrey, M. Brahlek, Y. Horibe, K. Iida, M. Tanimura, G.-H. Li, T. Feng, H.-D. Lee *et al.*, *Thin Solid Films* **520**, 224 (2011).
- [35] O. Mosendz, J. E. Pearson, F. Y. Fradin, G. E. W. Bauer, S. D. Bader, and A. Hoffmann, *Phys. Rev. Lett.* **104**, 046601 (2010).
- [36] K. Ando, and E. Saitoh, *Nat. Commun.* **3**, 629 (2012).
- [37] A. Azevedo, L. H. Vilela-Leão, R. L. Rodríguez-Suárez, A. F. Lacerda Santos, and S. M. Rezende, *Phys. Rev. B* **83**, 144402 (2011).
- [38] M. Harder, Z. X. Cao, Y. S. Gui, X. L. Fan, and C. M. Hu, *Phys. Rev. B* **84**, 054423 (2011).
- [39] L. Bai, P. Hyde, Y. S. Gui, C. M. Hu, V. Vlaminck, J. E. Pearson, S. D. Bader, and A. Hoffmann, *Phys. Rev. Lett.* **111**, 217602 (2013).
- [40] K. Ando, and E. Saitoh, *J. Appl. Phys.* **108**, 113925 (2010).
- [41] Y. Tserkovnyak, A. Brataas, and G. E. W. Bauer, *Phys. Rev. Lett.* **88**, 117601 (2002).
- [42] T. Gerrits, M. L. Schneider, and T. J. Silva, *J. Appl. Phys.* **99**, 023901 (2006).
- [43] N. Mecking, Y. S. Gui, and C. M. Hu, *Phys. Rev. B* **76**, 224430 (2007).
- [44] Z. Feng, J. Hu, L. Sun, B. You, D. Wu, J. Du, W. Zhang, A. Hu, Y. Yang, D. M. Tang *et al.*, *Phys. Rev. B* **85**, 214423 (2012).
- [45] X. D. Tao, Z. Feng, B. F. Miao, L. Sun, B. You, D. Wu, J. Du, W. Zhang, and H. F. Ding, *J. Appl. Phys.* **115**, 17C504 (2014).
- [46] T. Taniguchi, and H. Imamura, *Phys. Rev. B* **76**, 092402 (2007).
- [47] L. Liu, T. Moriyama, D. C. Ralph, and R. A. Buhrman, *Phys. Rev. Lett.* **106**, 036601 (2011).
- [48] J. Son, K. Banerjee, M. Brahlek, N. Koirala, S.-K. Lee, J.-H. Ahn, S. Oh, and H. Yang, *Appl. Phys. Lett.* **103**, 213114 (2013).
- [49] B. A. Assaf, T. Cardinal, P. Wei, F. Katmis, J. S. Moodera, and D. Heiman, *Appl. Phys. Lett.* **102**, 012102 (2013).
- [50] K. Fujiwara, Y. Fukuma, J. Matsuno, H. Idzuchi, Y. Niimi, Y. Otani, and H. Takagi, *Nat. Commun.* **4**, 2893 (2013).

Figure captions

Fig. 1. (a) Resistivity and carrier concentration of 20 QL Bi_2Se_3 as a function of temperature. (b) A schematic representation of spin pumping. (c) An illustration of the measurement setup. A rectangular $\text{Bi}_2\text{Se}_3/\text{Py}$ layer is patterned. An ACPS line is patterned on top of the SiO_2 layer. (d) Cross-section of the device. The layer stack is Bi_2Se_3 (t)/ $\text{Ni}_{81}\text{Fe}_{19}$ (20 nm)/ SiO_2 (30 nm), with $t = 5 - 35$ nm. The electrical contacts are Ta (5 nm)/Cu (150 nm).

Fig. 2. (a) Spin pumping induced ISHE signal (V_{ISHE}) measured at 4 GHz from the device with a Bi_2Se_3 thickness (t) of 20 nm, and in a bare Py (20 nm) film. The measured ISHE data (symbols) is fitted with a sum of a symmetric and an asymmetric Lorentzian. (b) Microwave photoresistance signals (ΔR_{MW}) at 4 GHz in the device with a Bi_2Se_3 thickness (t) of 20 nm. (c) The ratio of V_{ISHE} and resistance (R) of $\text{Bi}_2\text{Se}_3/\text{Py}$ films. (d) The FMR linewidth as a function of frequency for the Py and $\text{Bi}_2\text{Se}_3/\text{Py}$ films.

Fig. 3. (a) The spin Hall angle (θ_{sh}) and spin diffusion length (λ_{sf}) in Bi_2Se_3 as a function of temperature. (b) The measured magnetoconductance data (symbols) and corresponding fit (line) using Hikami-Larkin-Nagaoka (HLN) equation.

Fig. 4. (a) The spin Hall angle of Bi_2Se_3 surface and Bi_2Se_3 bulk, assuming a surface thickness of 3 nm, as a function of temperature. (b) The spin diffusion length of Bi_2Se_3 assuming different spin Hall angles in surface and bulk, as a function of temperature.

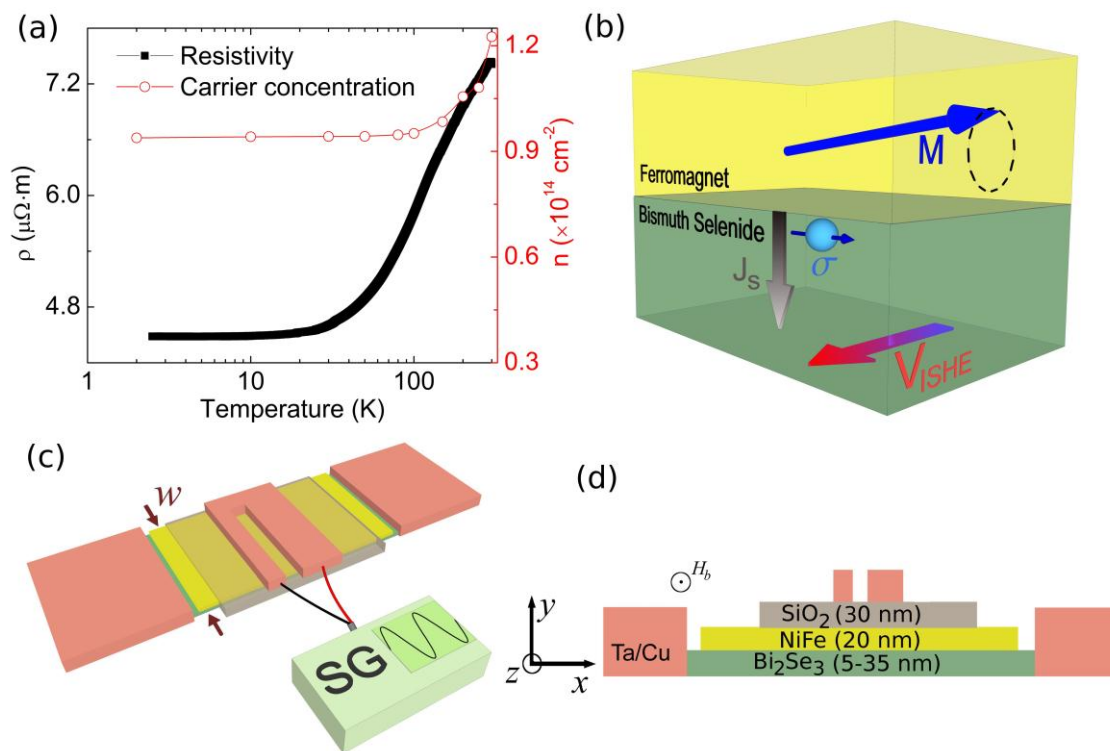


Fig. 1

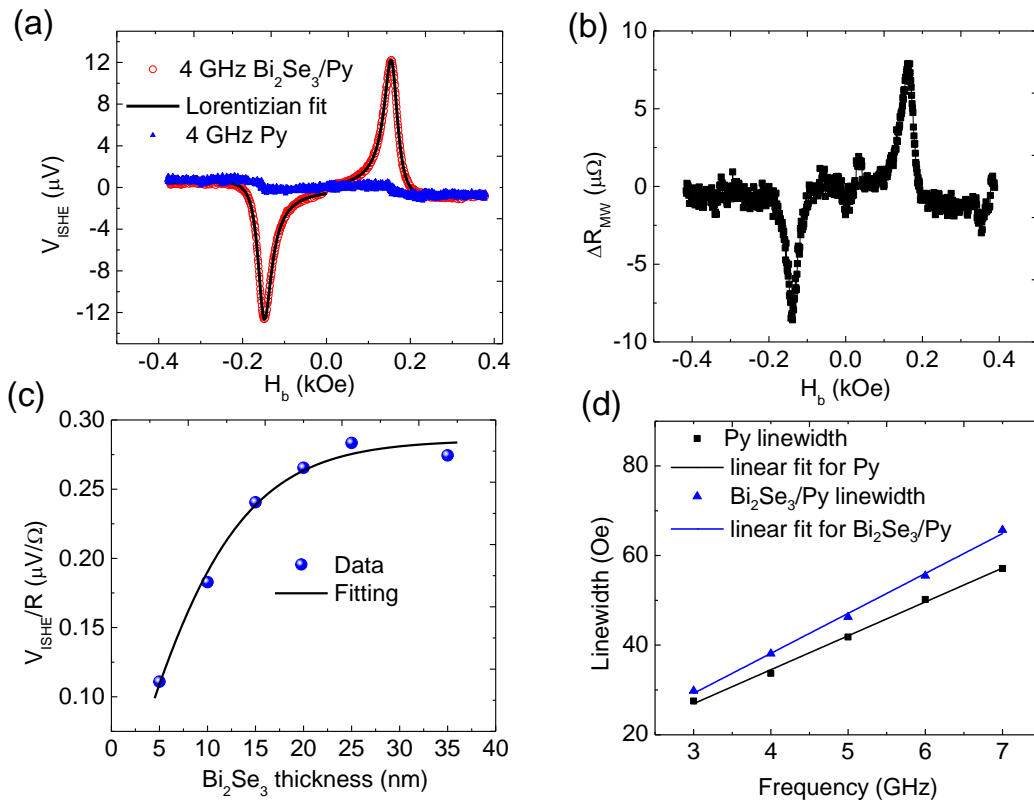


Fig. 2

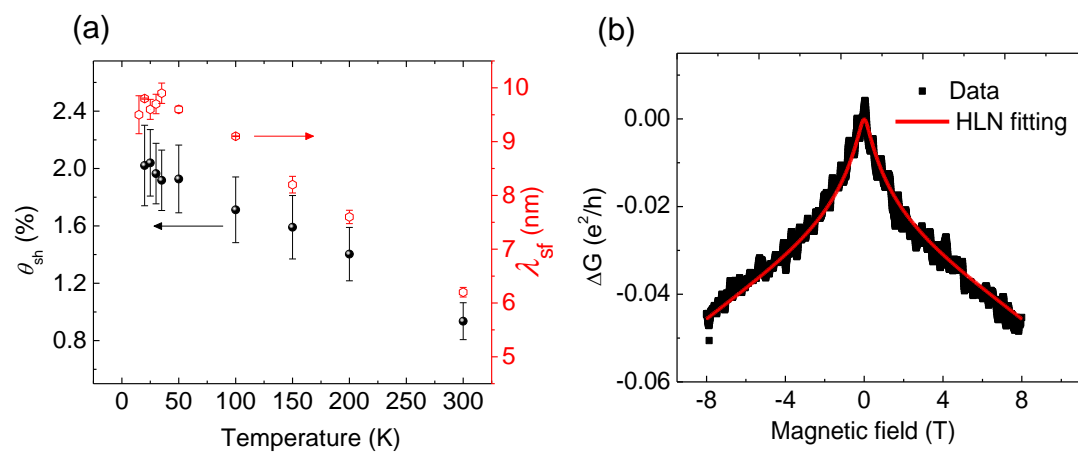


Fig. 3

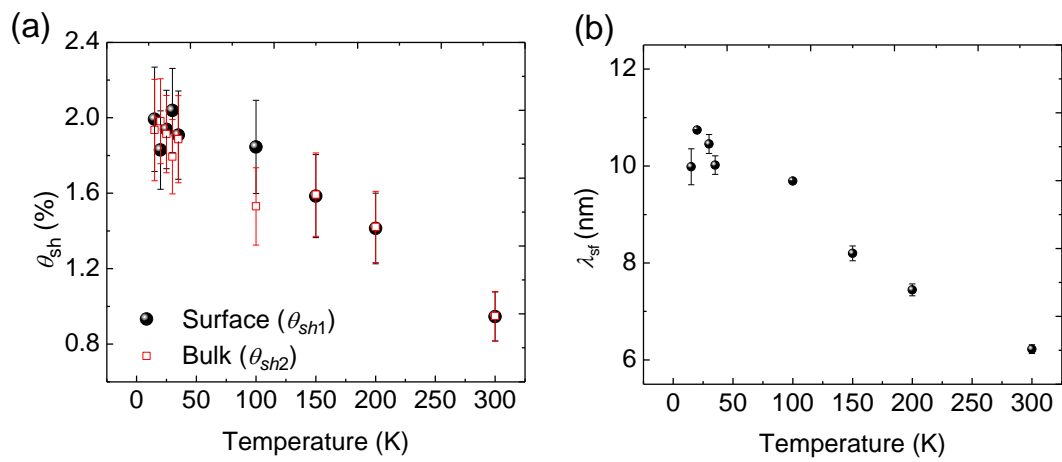


Fig. 4